Preparation of ZnS-CdS Nanocomposite for Photoelectrochemical Hydrogen Production

Jingyi Xu

Henan Polytechnic Institute, NO.666 Kongming Road, Nanyang, Henan, China.
E-mail: hnpi-jingyi@qq.com

Chalcogenide nanostructures and nanocomposites as semiconductors have attracted intense attentions in various potential applications such as hydrogen production owing to their remarkable photoelectrochemical activity. In this study, ZnS-CdS nanocomposite with cubic ZnS and hexagonal CdS was synthesized with a simple wet chemical method. As can be seen from SEM and TEM images, CdS was formed on the outer layer of ZnS NPs. The hydrogen production rate of ZnS-CdS nanocomposite was much higher than that of ZnS NPs, indicating the remarkable enhancement of hydrogen production activity of photocatalyst with the addition of CdS. The hydrogen production rate increased more than 4 times after the deposition of Ru on the surface of ZnS-CdS. In addition, the as-prepared ZnS-CdS nancomposite demonstrated an excellent stability over 50 h.

Keywords: ZnS; CdS; Photoelectrochemicallysis; Hydrogen; Nanocomposite

1. INTRODUCTION

With regard to the global energy demands in the long term, the sunlight to fuel conversion has attracted worldwide attention due to the limitation of fossil resources. Inspired by natural photosynthesis, the current fields of solar cell involve the development of system to capture and convert solar energy to chemical energy in the form of small but energy-dense molecules such as hydrogen. Since the first report of generation of H_2 and O_2 by photoelectrochemical splitting of water on TiO_2 [1, 2], various semiconductors such as celebrated TiO_2 have been developed as photoelectrochemical catalyst [3]. Among all studied semiconductors, ZnS has attained widespread interests owing to its relatively high catalytic activity for H_2 generation even in the condition without co-catalysts such as noble metal [4, 5]. The theoretical generation efficiency for photocarrier of ZnS was found to be much higher than that of TiO_2 due to the wide direct band gap of ZnS, leading to an

outstanding photoelectrochemical activity for ZnS. For instance, the photoelectrochemical degradation activity of ZnS nanomaterials with special morphologies was affirmed to be better than that of TiO_2 [6, 7]. For the sake of enhancing the photoelectrochemical activity of ZnS for hydrogen evolution, the modification of ZnS by various methods have been attempted to shift the light response of ZnS from ultraviolet region to visible region [8-10]. The coupling of ZnS with highly photo-sensitive CdS that possesses narrow band gap was verified to be an effective method. The photostability of ZnS was greatly improved, which could be attributed to the physical separation of ZnS from its surrounding medium and the prevention of photo-corrosion through reducing the number of dangling bonds on the surface of ZnS [8, 11]. However,the band gap with the ZnS is wider than CdS's ,the ZnS-CdS system exhibit more excellent performance better than single system about the band gaps.[12-20]. In our work, a simple wet chemical method has been employed for the preparation of ZnS-CdS nanocomposite catalyst and the obtained composite possessed a heterogeneous structure. The heterostructured ZnS-CdS catalyst has demonstrated to be a visible light-driven photocatalyst with remarkable performance such as improved photo-reactivity and photo-stability.

2. EXPERIMENTAL

2.1 Preparation of ZnS nanoparticles

All chemicals are analytical reagents supplied by Sigma-Aldrich, and used directly as received. *ZnS* nanoparticles were synthesized according to the recipe reported by Zhang [21]. 0.732 g of $Zn(AC)_2$ and 2 g of surfactant PVP was dissolved in 200 mL of water, and a clear solution was formed by stirring the mixture for 30 min. Similarly, 0.3 g of CH_3CSNH_2 (TAA) was dissolved in 100 mL of deionized water and the mixture was stirred for 30 min. Subsequently, the TAA solution was evenly added into PVP solution and the mixed solution was kept at 120°C in an oil bath for 1 h with constant agitation. After cooling down naturally to room temperature, the solution was treated with centrifugation. The obtained products were rinsed with water and ethanol for several times, and then dried at 80°C in vacuum oven.

2.2 Synthesis of ZnS/CdS nanocomposites

In a typical procedure, solution 1 was prepared by dissolving 0.732 g of Zn $(CH_3COO)_2$ and 2 g of surfactant PVP in 100 mL of component solvent containing deionized water and ethanol with equal volume. Solution 2 was synthesized by dissolving equal molar sodium sulfide in the same above-mentioned component solvent. Then solution 1 was added drop by drop into solution 2 and the mixture was stirred at 80°C until the formation of a homogeneous white solution. After 30 min, 50 mL of component solvent containing cadmium acetate with different concentrations was added drop by drop to the above solution and the reaction was carried out at room temperature. It was found that the color of solution was turned from white to green yellow after the addition of cadmium acetate. After 2 h, the formed yellow precipitate was collected by centrifugation and rinsed with deionized water and ethanol several times. Afterwards, 10 mL of water and ethanol component solvent containing zinc acetate with

the concentration of 0.5 M was added to the above colloidal solution. Then, the solution was kept stirring and sodium sulfide solution with the same molar amount was added drop by drop. Subsequently, the color of solution turned from green yellow into light yellow, indicating that the ZnS/CdS nanocomposite was successfully prepared. The result powder was washed and then dried at 80°C in oven.

2.3 Ruthenium deposition

In-situ photo-deposition was employed for the deposition of ruthenium (Ru) on the surface of ZnS-CdS catalyst. Specific experiment was performed by illuminating the CdSeZnS catalyst particles suspended in the acetic acid solution containing $RuCl_3$ for 20 min with 300 W Xe lamp (l > 420 nm). The calculated loading of Ru was approximately 5% based on the content of ZnS-CdS composite.

2.4 Characterizations

SEM and HRTEM images of the samples were collected with scanning electron microscope (Hitachi S-4800) and high-resolution transmission electron microscope (JEOL JEM-2100) with the acceleration voltage of 200kV, respectively. UV-vis spectrophotometer (Perkin Elmer Lambda 950) was employed for the optical analysis of obtained samples.

2.5 Hydrogen evolution measurements

A top-irradiation vessel interconnected by glass enclosed gas circulation system was used for photoelectrochemical water splitting. Reaction solution was prepared by dispersing the photocatalyst powder (100 mg) in 270 mL of aqueous solution containing Na_2SO_3 (0.1 M) and Na_2S (0.1 M) as the sacrificial reagents. A 300 W Xe lamp and cutoff filter of 400 nm were employed as the light source and visible light irradiation, respectively. The water splitting reaction was carried out at the constant temperature (20°C). The amount of H_2 evolved was determined by Shimadzu gas chromatography system.

3. RESULTS AND DISCUSSION

The SEM images of ZnS NP and ZnS-CdS nanocomposite were showed in Fig. 1A and Fig. 1B, respectively. The as-synthesized ZnS NPs were roughly spherical-like shape and the size was uniform with the average diameter of 97 nm. In contrast to the spherical ZnS NPs, the as-prepared ZnS-CdS nanocomposite was in flower-like shape, indicating that tiny CdS NPs was successfully deposited onto the surface of ZnS NPs. In addition, the average diameter of ZnS-CdS nanocomposite showed a slight increase (102 nm) compared with that of ZnS NPs (97 nm). TEM and HRTEM images were further collected to investigate the structure and morphology of ZnS-CdS nanocomposite. As

shown in the TEM image (Fig. 1C), solid spheres were observed. As can be seen form HRTEM image (Fig. 1D), an remarkable contrast was observed in the brightness between the inner and exterior layer of ZnS-CdS nanocomposite, indicating the successful formation of CdS on the outer layer of ZnS NPs. The interlayer lattice spacings of outer CdS phase was 0.331 nm, which matched well with the (111) plane of bulk cubic CdS.
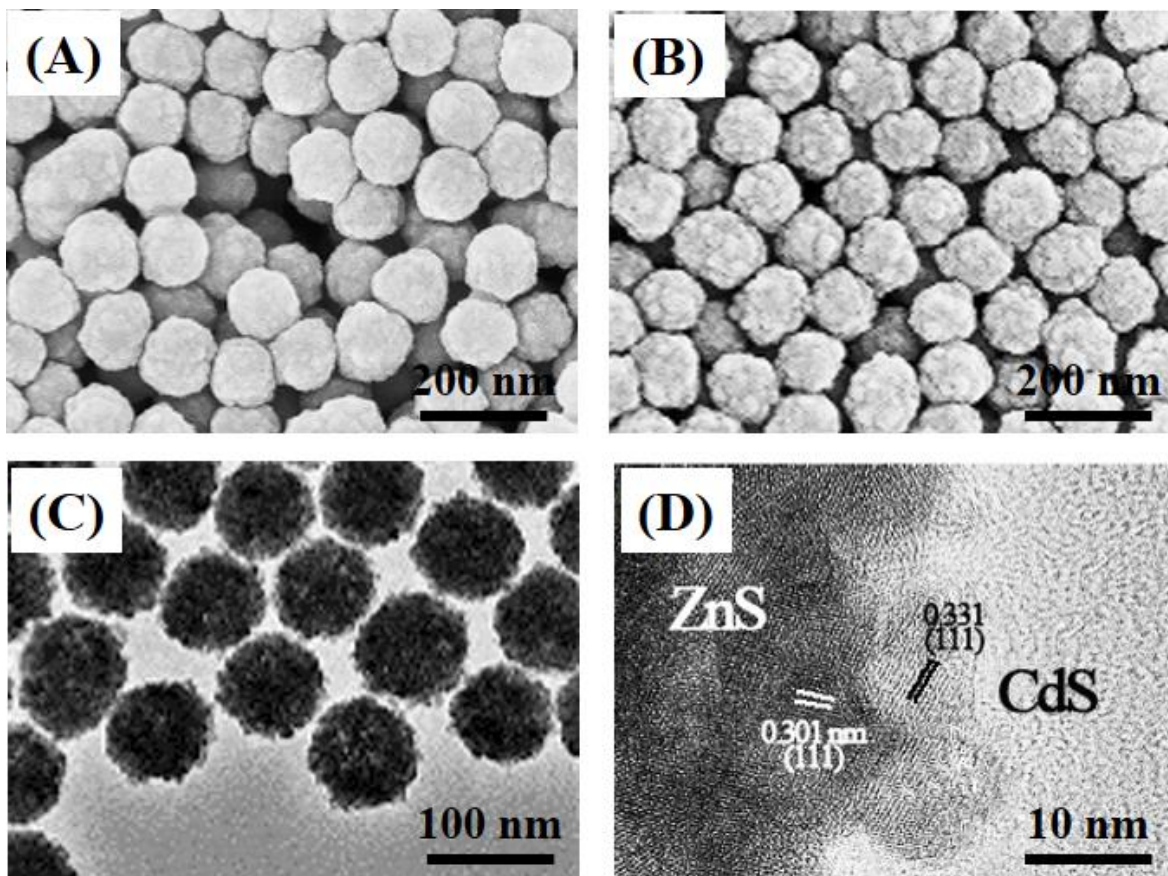
**Figure 1.** (A) SEM image of ZnS NPs. (B) SEM, (C) TEM and (D) HRTEM images of ZnS-CdS nanocomposite.

Fig. 2A showed the XRD spectrum of the obtained ZnS-CdS nanocomposite. The peaks at 2θ of 28.2°, 47.4° and 56.7° can be assigned to the (111), (220) and (311) planes of ZnS phase in face center cubic (JCPDS File No. 4-0783), respectively. Besides, the peaks at 2θ of 26.4°, 43.7° and 51.6° belong to the (111), (220) and (311) planes of CdS phase in face center cubic (JCPDS File No. 21-0829), repetively. All the observed peaks displayed a broadening, suggesting that the size of ZnS and CdS particles is small. It can be concluded from the XRD data that the composite consisting of ZnS and CdS phases was successfully prepared. The elementary composition of the ZnS-CdS nanocomposite was identified by EDX analysis. The EDX analysis was used for the investigation of elementary composition and the result was shown in Fig. 2B. Only Zn, S, Cd and O elements were observed in the EDX spectrum of ZnS-CdS nanocomposite. It was worth noting that the O signal could

be ascribed to the adsorbed O_2 in the powder sample. In general, the proposed wet chemical method was highly effective for the preparation of ZnS-CdS nanocomposite with high purity.
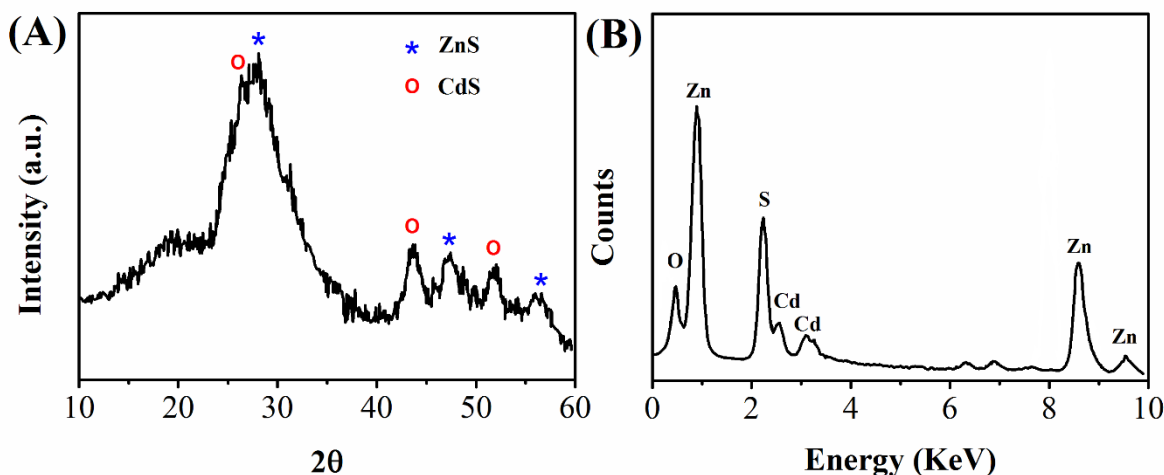
Figure 2. (A) XRD pattern and (B) EDX spectrum of ZnS-CdS nanocomposite.

Fig. 3A showed the UV-visible absorption spectra of ZnS NPs and ZnS-CdS nanocomposite. A strong visible light absorbance was observed in spectra of both ZnS NP and ZnS-CdS nanocomposite. The absorption peak of ZnS-CdS nanocomposite displayed a red shift in the visible light region when compared with that of ZnS NPs, which can be resulted from the loading of CdS NPs [22, 23].
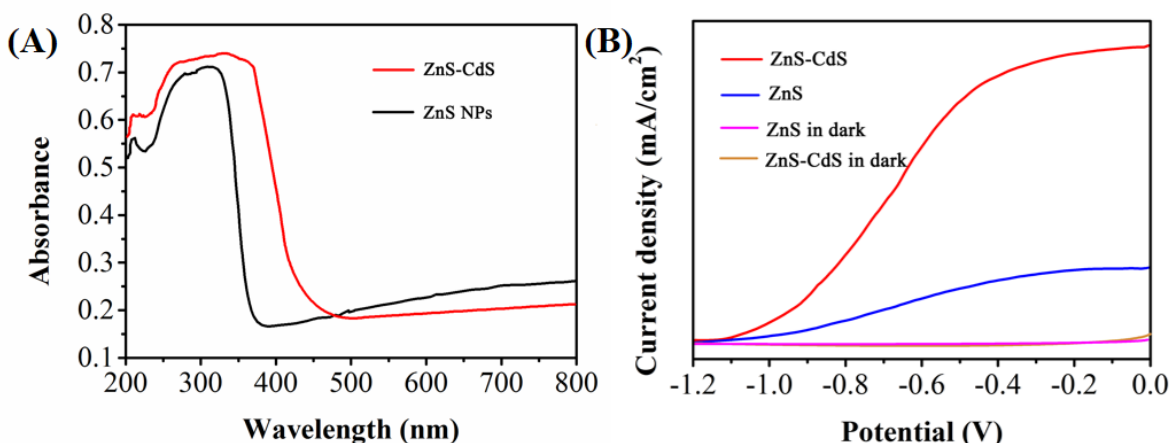

Figure 3. (A) UV-visible absorption spectra of ZnS NPs and ZnS-CdS nanocomposite. (B) Curves of photocurrent density in function of potential with ZnS NPs and ZnS-CdS nanocomposite as photoelectrodes in photoelectrochemical cells.

Linear-sweep voltammograms plots obtained on photoelectrodes fabricated with ZnS NP and ZnS-CdS nanocomposite were shown in Fig. 3B. For both ZnS NP and ZnS-CdS nanocomposite constructed photoelectrodes, the dark current was found to be very low as the potential ranging from -

1.2 V to 0 V (vs. SCE). In contrast to the obscure dark current, ZnS displayed a visible photo-induced current density at potential of -1.2 V and the photocurrent became more significant with the potential increased to -0.4 V. The highest photocurrent density was approximately 2 mA/cm^2 that obtained at potential of 0 V. It was found that the highest photocurrent density of ZnS-CdS nanocomposite (7.6 mA/cm^2) was greatly higher than that of ZnS NPs (2 mA/cm^2), indicating the significant improvement of photocatalytic activity by CdS NPs. The generation of bubbles on the surface of Pt electrode can be an indicator of high photocatalytic activity of as-synthesized ZnS-CdS nanocomposite as photoelectrode when applied for the hydrogen production from water in photoelectrochemical cell.

Nitrogen adsorption-desorption isotherms were performed to investigate the porous structure of the ZnS-CdS nanocomposite and the results were shown in Fig. 4. The calculated BET surface area was 31 m^2/g. As can be concluded form obvious hysteresis loop, the heterostructure pores existed in the as-prepared ZnS-CdS nanocomposite. The pore size distribution was obtained by the analysis of desorption isotherm by BJH method. The pore size of ZnS-CdS nanocomposite showed a distribution range of 4-16 nm, which greatly promoted the transport of reactant and product molecules across its pores.
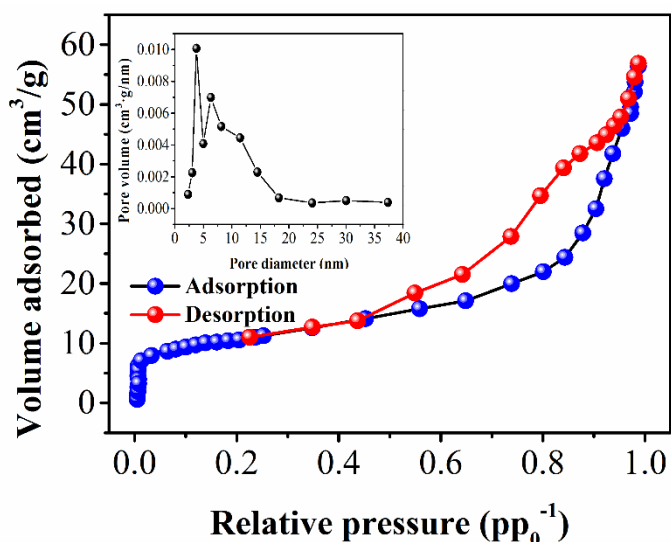

Figure 4. Nitrogen adsorption-desorption isotherms of ZnS-CdS nanocomposite. Inset showed the corresponding pore size distribution.

The hydrogen production rate of formic acid solution (10%) obtained on photoelectrodes constructed with ZnS NPs and ZnS-CdS nanocomposites under visible light were shown in Fig. 5A. It was found that the hydrogen production rate of ZnS NPs (25.1 mmol/h) was far lower than that of ZnS-CdS nanocomposite (157.5 mmol/h), indicating the remarkable enhancement of hydrogen production activity of photocatalyst with the addition of CdS. CdS is more photo-sensitive than ZnS, and thus the activity of photocatalyst composed of CdS can be significantly improved owing to the synergetic interaction between ZnS and CdS [24]. In addition, ZnS NPs play an important role in suppressing the recombination of the formed electron/hole pairs on CdS. Fig. 5B showed the stability of ZnS-CdS nanocomposite. As to ZnS-CdS nanocomposite, the hydrogen productivity remained 82%

after 10 runs when compared to the initial value. ZnS-CdS nanocomposite still possessed much higher hydrogen productivity than ZnS NPs after 10 runs, suggesting the higher stability of ZnS-CdS nanocomposite.
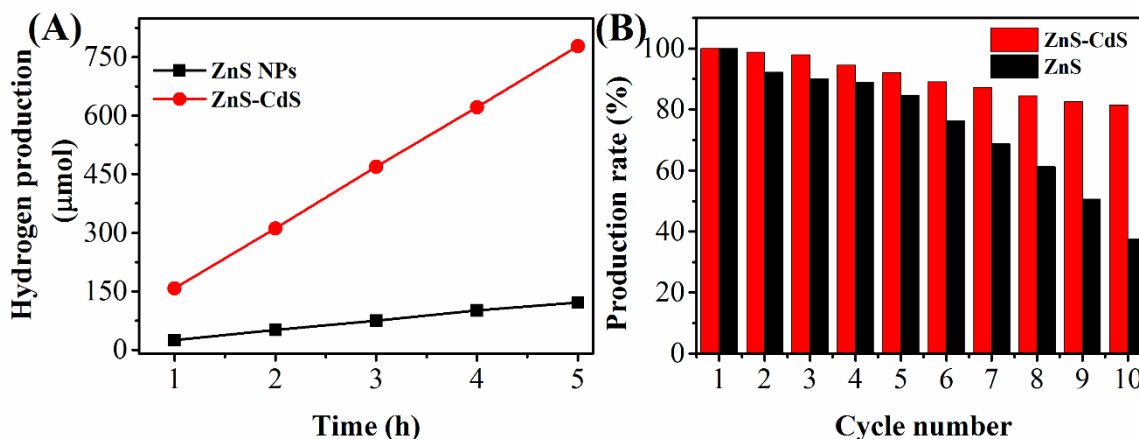
Figure 5. (A) Hydrogen production and (B) stability of the photoelectrodes constructed with ZnS NPs and ZnS-CdS nanocomposite.

The influence of deposited ruthenium on the performance of ZnS-CdS as photocatalyst was also studied. As can be seen Fig. 6, the hydrogen production rate showed 4 times increase after the deposition of Ru on the surface of ZnS-CdS. It was found that hydrogen could not be generated without the model organics for both ZnS-CdS and ZnS-CdS-Ru photocatalysts, which could be resulted from the function role of organics as electron donors during the H_2 evolution process catalyzed by various photocatalysts. Moreover, the influence of irradiation area and dosage of catalyst on the hydrogen productivity were also summarized. Both the obtained hydrogen production rates in methanol (154.9 mmol/m^2·h) and ethanol solutions (162.7 mmol/m^2·h) with ZnS-CdS photocatalysts were approximately more than 2 times higher than that with Ru/CdS/Al-HMS catalyst [25]. The hydrogen production rate in 10% methanol under light irradiation with ZnS-CdS photocatalysts was 5.5 mmol/g·h, which was nearly 12 times of that obtained with CuO/Al$_2$O$_3$/TiO$_2$ catalyst [26]. ZnS can be excited indirectly after the direct excitation of photo-sensitive CdS by visible irradiation, which can be ascribed to the promotion effect of excited CdS. The photo-excited electrons would drop from ZnS to CdS due to the more negative conduction band of ZnS (1.4 V) than CdS (0.3 V). And then the H$^+$ reduction occurred with the transfer of electrons from the conduction band of CdS to aqueous phase. Meanwhile, the electrons from chemical solution would transferred to the left holes at the valance band of ZnS, leading to the oxidation and degradation of organics.
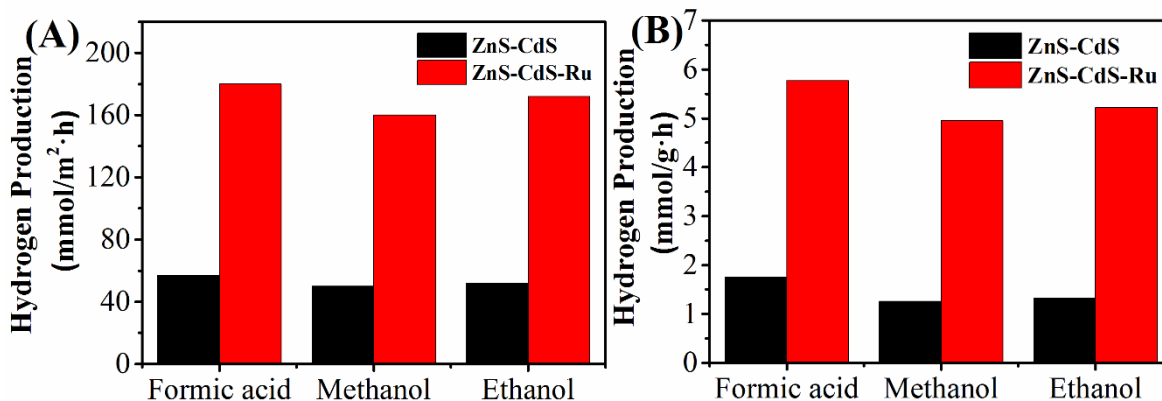
Figure 6. (A) The area-based and (B) weight-based specific hydrogen production rates in different model organic solutions under visible light with ZnS-CdS and ZnS-CdS-Ru as photocatalysts.

4. CONCLUSION

In conclusion, ZnS-CdS composite with heterostructure was prepared with the wet chemical synthesis method. As confirmed by SEM and TEM images, CdS layer was formed on the surface of ZnS NPs. The hydrogen generation rate under visible light obtained with the as-prepared ZnS-CdS as photocatalyst was approximately 4 times than that obtained with ZnS NPs. In addition, the hydrogen productivity performance of ZnS-CdS nanocomposite can be further improved with the addition of Ru.

References

1. A. Fujishima, *nature*, 238 (1972) 37
2. X. Xu, L. Hu, N. Gao, S. Liu, S. Wageh, A.A. Al-Ghamdi, A. Alshahrie and X. Fang, *Adv Funct Mater*, 25 (2015) 445
3. L. Fu, W. Cai, A. Wang and Y. Zheng, *Mater. Lett.*, 142 (2015) 201
4. J. Zhang, J. Yu, M. Jaroniec and J.R. Gong, *Nano letters*, 12 (2012) 4584
5. Y. Hong, J. Zhang, X. Wang, Y. Wang, Z. Lin, J. Yu and F. Huang, *Nanoscale*, 4 (2012) 2859
6. S. Xiong, B. Xi, C. Wang, D. Xu, X. Feng, Z. Zhu and Y. Qian, *Adv Funct Mater*, 17 (2007) 2728
7. J.S. Hu, L.L. Ren, Y.G. Guo, H.P. Liang, A.M. Cao, L.J. Wan and C.L. Bai, *Angewandte Chemie*, 117 (2005) 1295
8. K. Li, R. Chen, S.-L. Li, M. Han, S.-L. Xie, J.-C. Bao, Z.-H. Dai and Y.-Q. Lan, *Chemical Science*, 6 (2015) 5263
9. M. Jagadeeswararao, S. Dey, A. Nag and C. Rao, *Journal of Materials Chemistry A*, 3 (2015) 8276
10. D. Jiang, Z. Sun, H. Jia, D. Lu and P. Du, *Journal of Materials Chemistry A*, (2015)
11. Y. Tang, X. Hu and C. Liu, *Phys Chem Chem Phys*, 16 (2014) 25321
12. A. Kudo and M. Sekizawa, *Catal Lett*, 58 (1999) 241
13. J.-D. Huang, J.-Y. Liua and K.-L. Han, *international journal of hydrogen energy*, 37 (2012) e17881
14. G. Liu, L. Zhao, L. Ma and L. Guo, *Catalysis Communications*, 9 (2008) 126
15. G.G. Jang, C.B. Jacobs, I.N. Ivanov, P.C. Joshi, H.M. Meyer III, M. Kidder, B.L. Armstrong, P.G. Datskos, D.E. Graham and J.-W. Moon, *Nanotechnology*, 26 (2015) 325602

16. O.K. Echendu and I.M. Dharmadasa, *Energies*, 8 (2015) 4416
17. Y.-L. Wang, J.-T. Cao, Y.-H. Chen and Y.-M. Liu, *Analytical Methods*, 8 (2016) 5242
18. N. Qutub, B.M. Pirzada, K. Umar, O. Mehraj, M. Muneer and S. Sabir, *Physica. E*, 74 (2015) 74
19. H. Kumar, P. Barman and R.R. Singh, *Physica. E*, 67 (2015) 168
20. L.-x. ZHANG, H. XU, J.-q. ZHANG and W. LI, *Spectroscopy and Spectral Analysis*, 35 (2015) 320
21. Y. Li, Q. Li, H. Wu, J. Zhang, H. Lin, M. Nie and Y. Zhang, *Materials Science and Engineering: B*, 178 (2013) 135
22. M. Antoniadou, V.M. Daskalaki, N. Balis, D.I. Kondarides, C. Kordulis and P. Lianos, *Appl. Ctatl. B-Environ.*, 107 (2011) 188
23. G. QingáLu, *Chemical communications*, (2009) 3452
24. X. Wang, K. Shih and X. Li, *Water Science and Technology*, 61 (2010) 2303
25. Y.J. Zhang and L. Zhang, *Appl. Surf. Sci.*, 255 (2009) 4863
26. T. Miwa, S. Kaneco, H. Katsumata, T. Suzuki, K. Ohta, S.C. Verma and K. Sugihara, *International Journal of Hydrogen Energy*, 35 (2010) 6554